Distributed neural computation and the evolution of the first brains

Vikram Chandra[1,2], Mehrana R. Nejad[3,4], Allison P. Kann[1,2], Ananya Salem[1,2], Karl A.P. Hill[1,2,6], Richard Schalek[4], Jeff Lichtman[4], L. Mahadevan[1,3,5], Mansi Srivastava[1,2]

1. Department of Organismic and Evolutionary Biology, Harvard University, Cambridge MA 02138
2. Museum of Comparative Zoology, Harvard University, Cambridge MA 02138
3. School of Engineering and Applied Sciences, Harvard University, Cambridge MA 02138
4. Center for Brain Science, Department of Molecular and Cellular Biology, Cambridge MA 02138
5. Department of Physics, Harvard University, Cambridge MA 02138
6. Current address: Department of Biology, University of North Carolina at Chapel Hill, Chapel Hill NC 27599

Corresponding Authors: vchandra1@fas.harvard.edu, mansi@oeb.harvard.edu

Abstract

The origin of brains in the Precambrian was a landmark in animal evolution, enabling new behavior and life histories. Brains likely evolved from diffuse nerve nets, but we do not know what the first brains looked like or how they were organized. Acoel worms, the likely sister lineage to all other animals with brains, offer a unique window into this transition. Here, we studied the acoel worm *Hofstenia miamia*, a marine predator that hunts planktonic invertebrates and displays other sophisticated behavior. We found that *H. miamia* has an unusual 'diffuse brain': a subepidermal network of dense neuropil exhibiting little regionalization or stereotypy in gross anatomy or distribution of neural cell types. Remarkably, we found that behavior in *H. miamia* is robust to large, arbitrary amputations of brain regions, suggesting that most regions can perform most computations. More brain tissue improves performance, especially on challenging tasks, but no specific brain region is required. These results lead us to propose that *H. miamia*'s brain is composed of computationally pluripotent "tiles" that interact to generate coherent behavior. This architecture suggests a trajectory for nervous system evolution in which early brains may have arisen through the condensation of diffuse nerve nets into unregionalized brains, with regionalization evolving secondarily.

Main text

The evolution of brains was a milestone in the history of animals: it enabled new behavior, including early predatory lifestyles, and is thought to have triggered an evolutionary arms race between hunters and hunted that shaped the Cambrian explosion and modern animal diversity[1–5]. Modern animal brains are the result of this 'Cambrian information revolution'[5,6]. Although they vary substantially in their organization and complexity, brains are centralized computing organs

that serve as integrating centers; they collect sensory inputs and generate coherent organismal behavior[7–11]. Brains are highly regionalized, with specific regions specialized for specific tasks[12,13]. They are also stereotyped; within a species, all animals have the same brain organization. Brains evolved in the Bilateria (bilaterally-symmetric animals) some 550-600 million years ago, likely from ancient diffuse nerve nets[9,14,15]. Indeed, the first animal nervous systems were likely diffuse nets, and extant cnidarians (and possibly ctenophores) retain a version of diffuse nets[9,16]. Such nervous systems do not possess the core features of brains; for instance, they are not regionalized or stereotyped[17–19]. Instead, these features likely evolved during or after the origins of centralized nervous systems in bilaterians.

Over the last two centuries, much has been learned about the organization and function of diffuse nets. In the 1870s, Romanes and contemporaries, through a series of experiments involving incisions and amputations of jellyfish, first showed that cnidarians possess an unpolarized conducting substance distributed through their bodies[17,18,20]. A century later, electrophysiology and advances in histology reinforced these findings, and more recent work has begun to reveal detailed circuit explanations for how diffuse nets compute[21–27]. However, the large number of differences between diffuse nets and centralized brains has made it difficult for biologists to imagine what the first brains may have looked like, or how nets transitioned to brains[9,11,28].

Acoel worms are ideally poised to shed light on these questions. Acoels belong to the likely sister lineage to all Bilateria[29–32] (Fig. 1a). Moreover, acoels are thought to possess some of the simplest brains. In other words, their nervous systems appear intermediate between diffuse nets and centralized brains[11,33–37]. Comparing acoel brains to those of other bilaterians could reveal the architecture of ancient brains. However, acoel brains and behavior are poorly understood. Here, we study an acoel, the three-banded panther worm *Hofstenia miamia* (Fig. 1b). *H. miamia* lives in intertidal regions on beaches, mangroves, and salty lakes in the North Atlantic and Caribbean[9]. The worms are hermaphroditic and range in size from ~500μm to 1.5cm, and have relatively simple anatomy with a blind gut and few discrete organs[31,38,39]. Taxonomic descriptions suggest that the worms are “voracious predators”[38,40,41], and in recent work we found that they display complex reproductive behavior[42], suggesting they have a rich and sophisticated behavioral repertoire. We developed methods for quantitative analysis of *H. miamia*’s brain and behavior and found that *H. miamia* has a ‘diffuse brain’ that lacks the regionalization and stereotypy of well-studied bilaterian brains. We identify organizing principles for this diffuse brain, and suggest a trajectory for the evolution of the first brains.

The *H. miamia* brain lacks anatomical regionalization and stereotypy

In her taxonomic species description of *H. miamia,* Correa suggested that its brain was a subepidermal ‘ganglionic ring’ encircling the head[39]. Building upon this and recent work[36], we used a variety of imaging techniques (live dyes, immunofluorescence, and electron microscopy) to understand the brain at high resolution.

The brain contains a superficial network of dense neuropil, i.e., a structure composed primarily of neural projections, that lies peripheral to the body wall muscle and immediately

internal to the epidermis (Fig. 1c-e; Fig. S1a-c). Each ‘edge’ of the network contains neurites running in parallel. Superficial cellular patches tile the neuropil, and these often contain cells that coalesce into a sensory structure within each patch. These patches are composed of likely ‘H1’ receptors, sensory cells previously described in multiple acoels[43] (Fig. 1d; Fig. S1d), and also contain muscle cell bodies (Fig. S1e). The cell bodies of brain neurons lie ~30-50μm beneath the skin, internal to the body wall muscle. These cell bodies project outward into the neuropil, ~10-20μm below the skin (Fig. 1e-h). The two ‘layers’ of the brain are primarily composed of the same interneurons, with deep cell bodies generating neurites that project peripherally and coalesce into dense, superficial neuropil (Fig. 1h,i). The brain displays a slight dorso-ventral asymmetry: there are fewer network ‘edges’ in the neuropil near the ventral midline (Fig. S1a,b), possibly to accommodate the male copulatory apparatus[42].

With regards to cellular anatomy, we identified both unipolar and multipolar neurons in the brain (Fig. 1e,f). While the complete 3D structures of these neurons (and whether neurites are separable into distinct axons and dendrites) remain unclear, we found that they can have projections that extend well over 100μm (Fig. 1d; Fig. S1f). Sensory cells embedded in the skin project into the neuropil (Fig. 1e,g; Fig. S1g). Long cilia are visible near the mouth, likely corresponding to distinct sensory cell type(s) (Fig. S1a-c,h). Outside the brain, we detected multiple distinct innervated organs: the frontal organ (Fig. S1i), statocyst (Fig. S1j-l), penis (Fig. S1m), and pharynx (Fig. S1n). The brain itself connects to a sparse posterior network that extends through the body (Fig. 1c). Additionally, we found dense peripheral neural processes distributed through the skin (Fig. S1o; Video S1).

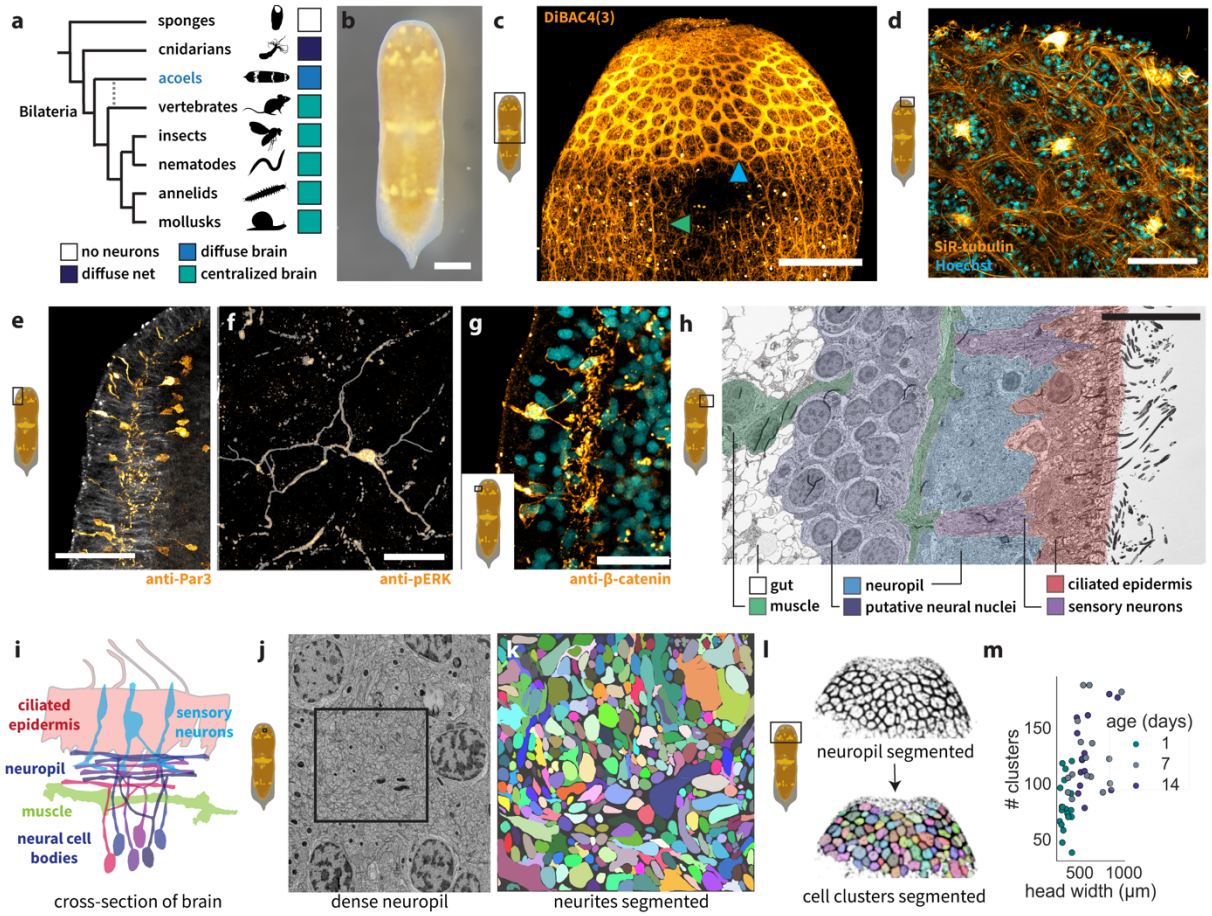

Figure 1: The organization of a diffuse brain. a) Simplified phylogeny of animals shows that acoel brains are likely intermediate between cnidarian diffuse nets and the centralized brains of typical bilaterians, with their alternative phylogenetic position annotated (dashed gray line). b) Photograph of juvenile *Hofstenia miamia*. c) Staining with voltage dye reveals a superficial network of dense neuropil (blue arrow) that extends into a sparser posterior nerve net (green arrow). d) Close-up view of neuropil stained sparsely with tubulin dye (orange) reveals that the neuropil (orange) contains many neurites running in parallel, with cellular clusters (cyan) interspersed between neurite bundles. Sensory neurons (likely clusters of H1 cells; bright orange) are set within many of these patches. e) Cross-section of brain stained with a Par3 antibody reveals that the brain has two layers: superficial neuropil, and deeper cell bodies that project outward. f) Staining with an ERK antibody (z-projected segmentation overlaid) shows that brain interneurons can be multipolar, with a central cell body generating multiple neurites. g) Cross-section of brain stained with an antibody against β-catenin reveals another sensory neuron class (possibly H2[43]) with two projections that innervate brain neuropil. h) Electron microscopy cross-section shows the fine organization of the brain, confirming the relative configuration of tissue types within the head. The superficial neuropil is visible immediately beneath the skin, while neural cell bodies lie deeper in the tissue, internal to body wall muscle (green). i) Schematic of cross-section of brain. j) Electron microscopy close-up of the brain shows dense neuropil; the box is a 6.7x6.7μm square. k) Segmenting neural projections within the highlighted box in (j) reveals over 400 neurites in a single section of neuropil. l) Segmentation of cellular clusters within neuropil allows quantification of brain structure and its variability. m) Quantifying the numbers of cellular clusters across brains reveals that, although cluster numbers increase with age (i.e. days after hatching) and size (i.e. head width, a good proxy for overall

body size[42]), worms vary widely in how many clusters they possess. Linear regression $p<0.0001$, $n=49$. Scale bars: 1mm (b), 200μm (c), 50μm (d,e), 20μm (f,g), 10μm (h).

H. miamia neuropil forms a network, with superficial resemblance to the diffuse nets of cnidarians and ctenophores. To understand the internal structure of *H. miamia* neuropil, we used electron microscopy. We found that every region of neuropil contains hundreds of fine, reticulated neural projections (Fig. 1j,k). This density is suggestive of complex connectivity and the likelihood that this brain harbors a diversity of circuit motifs. Importantly, this organization is fundamentally different from cnidarian or ctenophore nerve nets, which are typically 2-3 neurites wide[22,44,45], rather than hundreds or thousands of neurites wide.

Together, these results describe the structure of the *H. miamia* brain. Most remarkably, we found that this brain is virtually devoid of internal anatomical regionalization: within the neuropil, we detected no distinct regions, lobes, or stereotyped commissures. Regionalization is a core feature of typical bilaterian brains: across phyla as diverse as mollusks, arthropods, nematodes, vertebrates, and annelids, different brain regions have different structures and functions, and these regions are in the same relative positions across individuals within a species (and often over hundreds of millions of years)[12,46–48]. Given its lack of regionalization, the *H. miamia* brain appears to be fundamentally different. Next, we asked whether this brain displayed any stereotypy in its structure.

To test for stereotypy, we quantified brain structure by segmenting and counting the sensory patches that tile the neuropil (Fig. 1c,d,l). We found that as worms grow during juvenile development, the number of these patches increases (Fig. 1l,m). However, even among worms of the same age, size, and rearing environment, we found an order of magnitude of variation in the number of patches within their brains (Fig. 1m). Thus, while every brain has similar network topology, every brain is also different in its precise shape. This indicates that the same neural circuits cannot be in the same relative locations across worms. In other words, the *H. miamia* brain, unlike previously-studied bilaterian brains, appears to lack regionalization and stereotypy, and it suggests that this brain must be organized differently.

H. miamia **behavior is robust to large, arbitrary amputations of brain tissue**

The lack of anatomical regionalization within the *H. miamia* brain suggests that function may not be regionalized either. Taking advantage of *H. miamia*'s ability to survive substantial injury, we sought to assess functional brain regionalization by amputating brain regions and studying subsequent impacts on behavior.

To study the consequences of removing brain regions, we first developed an ethologically-relevant behavioral assay. *H. miamia* are thought to forage by hunting other small marine invertebrates in the wild, and they eat brine shrimp or rotifers in the lab. We developed a foraging assay in which worms are presented with a choice between a block of agarose containing prey rotifers and a control block of agarose containing no prey. We found that hungry worms navigated to the rotifers and attempted attacks (Video S2), while continuously fed (Fig. 2a-c) worms did not. Next, to ask whether this foraging behavior ceased when the worms had

167 consumed enough food: i.e., to ask whether hunger and satiety are opposing motivational
168 forces that regulate foraging behavior, we first starved worms and then fed them for 6h prior to
169 studying foraging. These sated worms did not forage, showing that foraging behavior in *H.*
170 *miamia* is motivation-dependent as in typical bilaterians[49] (Fig. S2a).
171 Next, we asked how foraging behavior was affected by amputating brain regions. First,
172 we performed a transverse amputation to separate heads from tails in starved worms. We found
173 that tail fragments, which lack brains, did not forage and were unable to move (Fig. S2b), while
174 head fragments foraged normally both immediately after amputation and two days later (Fig.
175 2d), when their wounds had closed but before their tails had regenerated[31,50]. This shows that
176 the posterior nerve net does not independently generate coherent movement or induce goal-
177 directed behavior, and that the brain is likely necessary for coordinated behavior. We then
178 removed the right half of the head (Fig. S2c). Worms missing half their heads did not display
179 obvious movement defects (Fig. S2d). More importantly, we found that two days after
180 amputation, worms missing half their heads foraged similarly to intact worms, when the wound
181 had closed but new tissue had not yet emerged (Fig. 2e; Fig. S2e-g,i,j). Similarly, removing the
182 dorsal half of the head, or the left half of the head, did not affect foraging two days after
183 amputation (Fig. 2e; Fig. S3a).
184 This robustness to amputation could result either from the inherent structure of the *H.*
185 *miamia* brain, or through rapid regeneration after injury. We found that worms missing half their
186 heads foraged successfully immediately after amputation (Fig. S3b), suggesting that foraging
187 behavior does not require regeneration of missing brain tissue. To confirm this finding, we
188 irradiated worms, ablating their pluripotent stem cells and thus inhibiting regeneration[31]. Worms
189 without stem cells foraged successfully regardless of whether their heads were intact or had
190 been amputated (Fig. S3c). These data show that robustness to amputation is an intrinsic
191 property of the *H. miamia* brain.
192 We next asked whether this robustness extended beyond the specific computations and
193 movements involved in the approach phase of foraging. To study the capture phase of foraging,
194 we provided worms access to a controlled density of free-moving rotifers for a defined time
195 period, and quantified the number of rotifers they consumed. Worms missing half their heads
196 consumed similar numbers of rotifers to intact starved controls (Fig. 2f). These data show that
197 amputation of large fractions of the brain do not prevent worms from executing the set of tasks
198 necessary for foraging. In addition, these amputations include conditions in which the statocyst,
199 frontal organ and associated neurons were damaged or entirely removed, showing that these
200 organs are dispensable for all aspects of foraging behavior.
201 Next, to further test the generality of brain robustness, we removed wedges of differing
202 sizes from the heads of worms: a small wedge, two bilateral wedges (to account for the
203 possibility of bilaterally-symmetric, specialized regions with redundant roles), and a large wedge
204 that removed the majority of the head (Fig. S3d; Video S3). We found that worms foraged
205 robustly despite the loss of these brain regions (Fig. 2g). In many of these conditions, wound
206 closure involves the attachment of dorsal and ventral wound edges[50], likely connecting brain
207 regions that are normally separate (Fig. S2g). Despite these abnormal structural configurations,

208 worms displayed robust foraging behavior. Moreover, analysis of the angular distributions of the
209 trajectories of these worms found no major differences across treatments, and no turn bias,
210 even after large lateralized amputations (Fig. S3e). This shows that most or all regions of the *H.*
211 *miamia* brain can locally perform motor control. Finally, we also conducted a wide variety of
212 additional amputations, removing wedges of varying size and location from worm heads. These
213 also did not affect foraging behavior (Fig. S3f).
214 While removing large amounts of brain tissue did not affect foraging, we found that
215 removing the mouth did inhibit successful foraging (Fig. 2e; Fig. S2h). These worms have no
216 obvious movement defects (Fig. S2d). Worms missing their mouths consumed fewer rotifers
217 than intact worms or those missing half their heads, but significantly more than intact fed worms
218 did (Fig. 2f), suggesting that the mouth is not strictly necessary to assess internal nutritional
219 state, or to coordinate goal-directed appetitive or consummatory foraging behavior. Together,
220 these data suggest that amputation of the mouth may result in a chemosensory-specific defect,
221 consistent with the presence of specific sensory cell types near the mouth (Fig. S1a-c,e)[43], and
222 indicate that robustness is a feature of brain computations downstream of chemosensation.

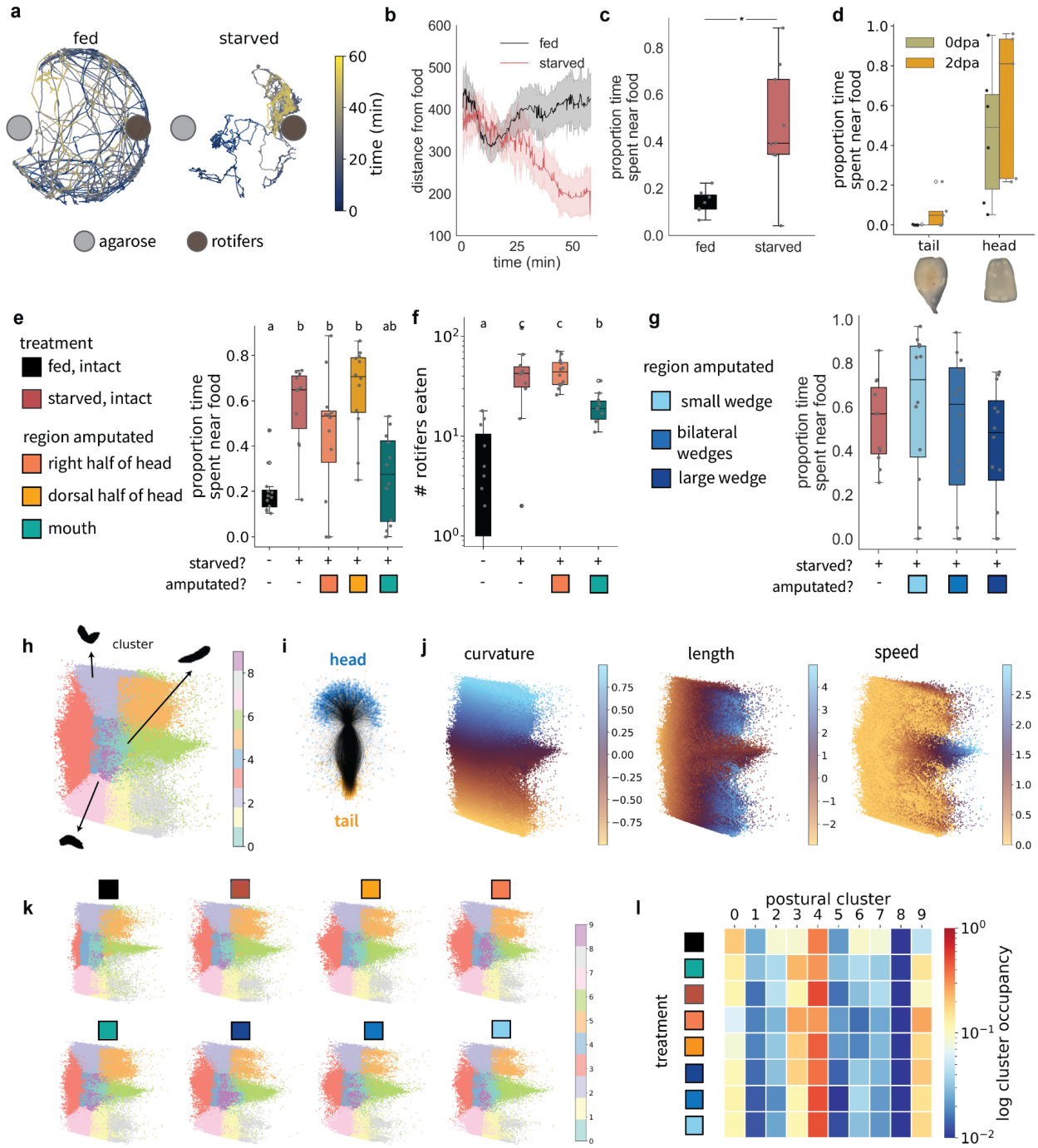

Figure 2: *H. miamia*'s foraging behavior is robust to brain amputations. a) Examples of tracks for a representative fed and starved worm presented a choice between agarose blocks with and without rotifers. Trajectories colored by time. b) Starved worms approach the rotifers; fed worms generally do not (see also Fig. S3a). Error band represents standard error. c) Quantifying this behavior as the proportion of time spent near food provides a robust metric of foraging behavior (see Methods); t-test FDR-corrected p=0.03,n>=6, data also used in Fig. S3a. d) Amputated tails do not forage, either immediately (0 dpa: t-test p=0.01, n>=5) or two days after (2dpa: t-test p=0.01, n>=5) amputation, while amputated heads do. e) Amputation of the right or dorsal half of the head does not affect foraging behavior, while amputation of

the mouth inhibits foraging. f) Quantifying the number of rotifers in the guts of worms shows that amputation of half the head does not affect feeding. Letters above boxplots in (e) and (f) indicate significance levels after one-way ANOVA and Tukey post-hoc tests; corrected ps<0.05. g) Removing tissue of varied size and geometry from the brain also does not affect foraging behavior. One-way ANOVA p=0.54, n>=10. h) A low-dimensional postural space (i.e. of the first two principal components of the space defined by curvature, length, and speed) captures major elements of *H. miamia*'s postures during foraging, with k-means cluster identities shown, and representative worm postures overlaid for some clusters. See Table S1 for mean values of curvature, length, and speed for each cluster. i) Overlaid and aligned splines fitted to tracked worm midlines from a representative worm show the space of possible postures - and especially curvature - for a worm. j) Normalized curvature, worm length (z-scored within worm), and speed appear as gradients within the postural space. k) Projecting amputated worm postures into this postural space shows that irrespective of amputation, all worms express all elemental postures. l) Comparing postural cluster occupancies shows that fed, intact worms are most different in their postural behavior, while amputated worms generally display only minor differences in occupancy compared to starved, intact worms. Legend for treatment colors in (e) and (g). See Tables S2 and S3 for statistics.

Overall, these data show that behavior in *H. miamia* is remarkably robust to the removal of large, arbitrary majorities of brain tissue. Nonetheless, it is possible that worms with amputated brain regions experience some subtle behavioral defects. We reasoned that these hypothetical defects may be observable in their motor coordination, since the worms were clearly able to detect prey, to sense their internal state, and to select actions necessary for foraging. We therefore quantified worm posture during foraging at high resolution, by tracking keypoints on the worm's midline. Using these data, we generated a low-dimensional postural space during foraging from starved worms with intact brains (Fig. 2h-j; see Methods). The boundaries of the occupied region of this space (Fig. S4a) reveal core biomechanical constraints on *H. miamia*'s movement. *H. miamia* has two motor systems: epidermal cilia (Fig. 1h, Fig. S1h) polarized along the anterior-posterior axis beat to produce thrust and allow forward gliding, and distributed groups of muscle (including an orthogonal grid of body wall muscle) contort to allow turning (Fig. 1h)[51]. Worms in sharp turns experience no forward displacement, likely because the cilia in different body regions are beating in different directions. Worms are fastest when at intermediate length, but stretch and compress themselves frequently (Fig. S4a).

Next, we used k-means clustering to segment elemental postural states within this space (Fig. 2h; Table S1). We then projected onto this space similar data from fed worms with intact brains as well as starved worms subjected to numerous amputations (i.e., data from Fig. 2f,g). We found that fed, intact worms were most different in their postural expression, consistent with their lack of foraging behavior (Fig. 2k,l; Fig. S4b,c; Table S2,3). Arbitrary amputations of brain regions did not affect the generation of postures or the transitions between postures, although we detected small but significant effects on relative occupancy of specific postural states and transitions (Fig. S4b,c; Table S2,3). In addition, our postural analyses did not detect differences in turning bias after amputations of the right half of the brain (Fig. 2k,l; Table S1,2; Video S3). This reinforces the idea that brain regions locally generate postural states necessary for both

left and right turns (along with all other motor commands), unlike in typical bilaterians where a specialized brain region commands distant motor systems, frequently in a lateralized manner[52,53]. In other words, these data suggest that most or all motor commands can be generated in any or all brain regions, control motor behavior locally, and can be transmitted body-wide.

Together, these data show that the *H. miamia* brain exhibits little functional regionalization. Instead, most or all brain regions are computationally pluripotent, i.e., most or all neural computations necessary for foraging occur in many or all regions of the brain, likely simultaneously. These computations include sensory processing and integration, internal state assessment, selecting actions, and motor control of most or all muscular and ciliary motor systems, i.e., the generation of all static postures and their sequences.

Neural cell types lack regionalization within the brain, consistent with a tiled organization

How might such a brain be organized? We hypothesized that the brain is composed of tiles of similar neural circuits, each of which is computationally 'pluripotent'. If this were true, we would expect these tiles to be composed of ensembles of similar neural cell types. Conversely, detecting substantial regionalization in the locations of individual cell types would disprove this hypothesis. Our previous work in *H. miamia* found that neural markers are distributed across the entire brain[54,55]. However, many of these markers are expressed in large subsets of neural cell types, and we reasoned that, as in typical brains[56,57], markers of sparse cell types could exhibit greater regionalization. To test the tiling hypothesis more directly, we therefore sought markers of sparse cell types. We first integrated all relevant *H. miamia* single-cell RNA sequencing datasets[54,58] (Fig. S5a), selected all neurons (Fig. S5b,c), and reclustered them to identify individual neural cell types (Fig. S5d,e). Analyzing this dataset of 15,262 cells, we identified 25 putative neural clusters with specific markers for most clusters (Fig. 3a). We selected markers likely to have functional relevance from this list. To overcome the possibility that some neural markers may not be represented in this dataset due to technical limitations, we also included evolutionarily conserved genes with likely roles in neurotransmitter synthesis or processing pathways that were previously identified[59–61].

We used fluorescence *in situ* hybridization to assess the distribution of neurons expressing these genes in worms. Of 44 genes that we screened (Table S4), we identified 21 with expression in the brain, including several that labeled sparsely-distributed neurons within the head and others that labeled large subsets of neurons (Fig. 3b; Fig. S6). Qualitatively, all identified cell populations appeared largely or entirely distributed across the brain, regardless of their density (Fig. S6). To systematically test regionalization, we quantified gene expression patterns for all markers in the head (including for previously published markers for all qualitative neural expression classes, but excluding markers of sensory neuron populations in the mouth and elsewhere in the body), and we computed two density-corrected indices of regionalization for each gene (Fig. 3c; see Methods). Irrespective of their sparseness, markers had minimal regionalization on both indices (Fig. 3d). These data are consistent with the tiling hypothesis. Taken together, our anatomical, behavioral and molecular data all find little evidence that the *H.*

miamia brain contains specialized regions. Instead, the brain may be composed of repeating, computationally pluripotent units - which we term ‘circuit tiles’.

The exact wiring architecture of circuit tiles remains unknown, but our data suggest some constraints on their organization. It is possible that the patches of sensory cells that tile the brain, with surrounding neuropil, represent computationally pluripotent circuit tiles themselves. However, some cell type markers are sparser than these (e.g. *th, hnmt2, unknown-235* - see Fig. 3d; Fig. S6). Since tiles are pluripotent, and if we assume these sparse cell types are necessary for some computation, it would follow that each tile must contain at least one representative of each cell type. Therefore the patches of sensory clusters are unlikely to be the pluripotent circuit tiles. It would further follow that the size of each tile is set by the distance between neighboring cells of the sparsest type. Alongside these constraints, it is possible that tiles vary in their exact composition and architecture. Tiles need not occupy entirely discrete regions of space; it is possible that they overlap partially. We also do not wish to imply that tiles necessarily have higher within-unit than between-unit connectivity; in fact, our anatomical studies of the brain (e.g. Fig. 1d) suggest that there is likely extensive lateral connectivity across all regions of the neuropil. Regardless, the worm’s anatomy ensures that every tile contains connections to the motor systems: epidermal cilia, peripheral, body wall, parenchymal and pharyngeal muscle. In addition, tiles likely contain one and possibly multiple sensory cells or organs, which allows each tile to locally receive some sensory input and to transmit most or all motor commands (Fig. 1i).

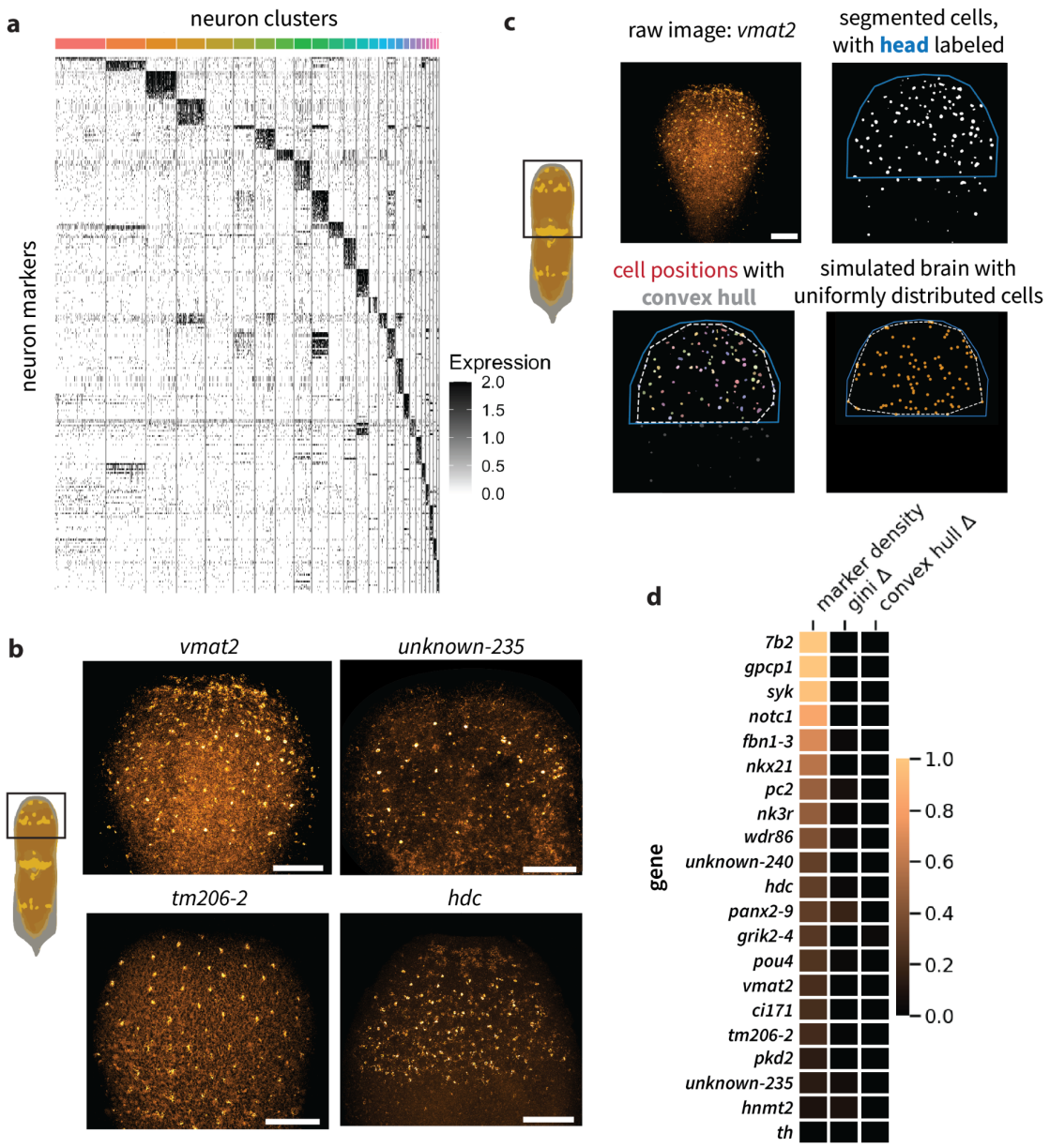

Figure 3: Neural cell types are distributed across the *H. miamia* brain. a) Heatmap of top 20 markers from each neural cluster shows that many markers are expressed in specific clusters, suggesting that these are cell-type specific markers. b) Fluorescence in situ hybridization of neural markers reveals that several (e.g. *vmat2*, *unknown-235*, *hdc*) label sparse, distributed populations, while others are expressed broadly (e.g. 7b2). c) Outline of analysis of spatial distributions of markers: pixel classification to segment fluorescent puncta (corresponding to cell bodies for sparse markers), fitting convex hull to segmented cells and calculating the ratio of its area to the area of the polygon describing the brain, and simulating brains with uniformly distributed cells with the same density as the empirical data. d) Neural markers exhibit little regionalization across a wide range of cell densities, as assessed by two metrics: the difference in gini coefficients for brain regions containing expression between real brains and simulated uniform brains, and the difference in the proportion of brain area containing cells between real brains and simulated uniform brains. Scale bars: 100μm.

On how a diffuse brain computes

The unusual organization of the *H. miamia* brain raises several questions. For instance, why does it contain multiple circuit tiles, when fewer, or perhaps even one, should do? We reasoned that while no specific brain region may be necessary for any computation, more circuit tiles may allow better performance. To seek associations between available brain area and behavior, we first reanalyzed the experiment in which we amputated different amounts of brain tissue (Fig. 2g). Analyzing these data as a function of approximately how much brain tissue was removed (rather than as a set of discrete perturbations), we found that although no amputation treatment prevented worms from foraging successfully, worms missing more brain tissue took slightly longer to find immobilized rotifers (Fig. 4a; Fig. S7a). This was not because the worms were mechanically impaired or took longer to travel the same distance (Fig. S7b); instead, worms missing more brain tissue may be worse at locating prey. To test whether this effect was reproducible, we diluted the prey stimulus by reducing the concentration of immobilized rotifers presented to the worms, making it more challenging for worms to locate prey. Worms missing ~80% of their brains successfully located rotifers when presented a high concentration, but not when presented a low concentration (Fig. 4b), suggesting that more brain tiles may allow greater perceptual resolution and therefore behavior resulting in higher fitness. These results also showed that presenting the worms with challenging tasks can reveal subtle effects of amputation.

To conclusively test the idea that more tiles allow better estimation of prey position, and to identify any other subtle effects of amputation, we sought to challenge the worms in a more dramatic, and ethologically-relevant way. We studied the hunting behavior of worms pursuing a single free-moving prey (i.e. a brine shrimp) - a challenging task in which nearly all hunts end in failure to consume the prey within the duration of the assay (we recorded 1/12 successful captures among intact worms in one experiment). We jointly tracked the positions of the worm and the shrimp (Fig. 4c, Video S4). Shrimp had lower velocity autocorrelations when in the presence of a worm (Fig. S7c), suggesting that they actively evade being hunted. Similarly, worms displayed lower velocity autocorrelations when the shrimp was present (Fig. S7d), showing that they actively hunt escaping prey. Worms with half their heads amputated displayed similar dynamics, but had slightly lower velocity autocorrelations compared to intact worms, specifically during foraging (Fig. S7d). These data suggest that amputation has a subtle impact on how worms hunt, but has little impact on the worms' ability to detect stimuli or execute movements. We therefore asked whether amputated worms are worse at hunting.

We found that worms were able to track shrimp, moving towards the trajectory of the shrimp, with the worm lagging the shrimp by 20-30 seconds (Fig. 4c,d; Video S4). Worms missing half their heads were poorer at tracking shrimp (Fig. S7e). Next, in another cohort of worms, we removed increasing fractions of brain tissue and analysed postural dynamics and hunting behavior. This experiment, done in a richer behavioral setting, confirmed our previous finding that all postures and postural sequences are robust to large-scale amputation, and can be generated by arbitrary brain regions (Fig. S7f-j). Indeed, relative occupancy of postural states, and transitions between postures, were also largely indistinguishable between intact and

amputated worms (Fig. S7i,j, Table S5,S6). However, we found that worms missing greater fractions of brain tissue displayed poorer tracking (Fig. 4d). In principle, this could be explained by the fact that some amputations also remove fractions of their mouth, and could reduce chemosensory sensitivity. To control for this possibility, we repeated this experiment, removing varying fractions of brain tissue but leaving the entire mouth intact in all cases. Again, worms missing greater fractions of brain tissue displayed poorer prey tracking (Fig. 4e), confirming that prey tracking is sensitive to the loss of brain tiles downstream of sensation. These data show that more brain tiles allow greater perceptual resolution.

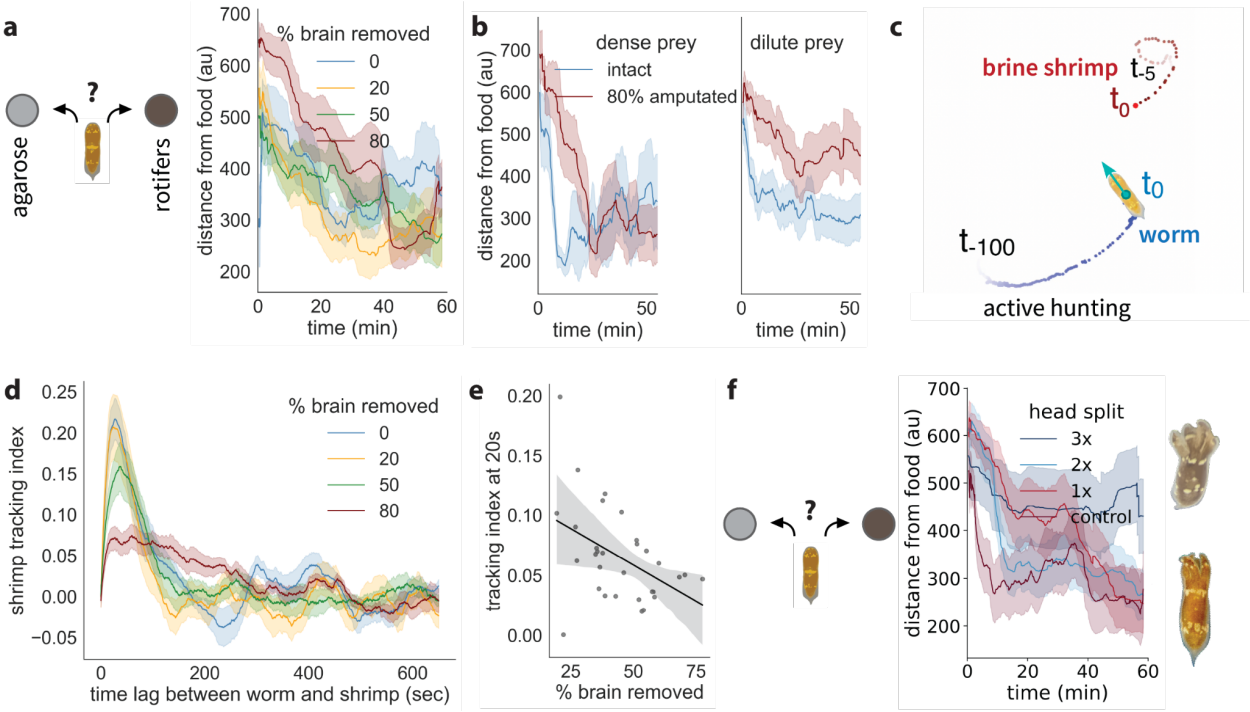

Figure 4: The collective behavior of circuit tiles. a) Worms missing greater fractions of their brain take longer to locate rotifers embedded in agarose (schematic shows assay design: worms choose between agarose containing rotifers and plain agarose, as in Fig. 2). b) Reproducing this effect, worms with ~80% of their brain missing are unable to detect a low density of rotifers embedded in agarose, and are slower to detect rotifers at high density. High-density prey, intact vs amputated t-test for proportion of time spent near food: p=0.8, n=5 per treatment. Low-density prey, intact vs amputated t-test for proportion of time spent near food: p=0.02,n>=14 per treatment. c) Schematic of hunting behavior assay, showing joint tracking of worm and its prey shrimp. The recent trajectory of the shrimp is shown in red (5s); the recent trajectory of the worm is shown in blue (100s). The cyan arrow shows the direction of motion of the worm. d) Worms track shrimp positions; worms missing more brain tissue display poorer tracking. Linear regression of max. tracking index: p<0.0001, n=38. e) Worms missing more brain tissue display poorer tracking, even when their mouths are completely intact. Linear regression of tracking index at a lag of 20s: p=0.01, n=31. f) Splitting the brain into six fragments inhibits foraging behavior one hour after incision, with worms unable to detect rotifers embedded in agarose. Tukey post-hoc tests for mean distance from food at the end of the assay, 3x vs other treatments p<=0.02, n>=9 per treatment. All error bands represent standard error.

Finally, we asked how brain tiles collectively generate coherent organismal behavior. One possibility is that brain tiles compute independently, with the motor systems effectively summing their separate outputs: i.e., the *H. miamia* brain would perform degenerate computations. Alternatively, it is possible that tiles interact, allowing computations to emerge from their collective activity: distributed computation. To test this hypothesis, we split heads into increasing numbers of fragments. Each fragment remained attached to the body; i.e. the number of brain tiles stays constant. We reasoned that this would disrupt interactions between brain tiles, but allow them to generate motor outputs independently. Consistent with this hypothesis, worms with their heads split into two or four fragments foraged similarly to intact worms, but worms with their heads split into six fragments did not (Fig. 4f). These worms were capable of coordinated movement, indicating that this defect was not mechanical (Video S5). Together with our anatomical data showing extensive lateral connectivity (Fig. 1d; Fig. S1d), this suggests that circuit tiles do indeed interact, with coherent organismal behavior emerging from the collective activity of interacting brain tiles.

Conclusion

Nearly a century ago, Lashley lesioned cortical regions from the brains of rats, and found that they could still perform spatial navigation and solve mazes[62,63]. From these and earlier experiments, he devised principles for brain organization: the principle of equipotentiality (effectively: brain regions are computationally pluripotent - or equipotent) and the principle of mass action (effectively: more brain is better). However, further work showed that Lashley's principles do not accurately describe the organization of mammalian brains, which are indeed regionalized[13,64–66]. Strikingly, our results show that *H. miamia*'s diffuse brain, unlike typical bilaterian brains, does obey Lashley's principles. We find that the *H. miamia* brain is not regionalized anatomically, cellularly, or functionally, and that all brain regions appear to perform most or all neural computations. We propose that the brain is composed of tiles of pluripotent neural circuits, and that these tiles interact to implement distributed computations. More generally, our results suggest that the space of realized brain forms may be broader than was previously assumed; brains do not have to be highly regionalized or stereotyped.

The precise historical sequence of the transition from nets to brains remains unknown, and is highly debated[9,10,67]. It has been proposed that ancient sensory organs connecting to diffuse nets served as nucleation centers for nascent brains[9,68]. In this view, the first brains would have been at least somewhat regionalized internally. Our work raises another possibility. We suggest that diffuse brains lack regionalization, and that the first brains may have retained the ancestral lack of regionalization and stereotypy that typifies diffuse nets. Perhaps these nascent brains then evolved elaborations for dense connectivity, new molecular signaling systems[59], and possible new neural morphology and circuit motifs[46,69] - coalescing in new behavioral affordances. Regionalized, stereotyped circuits may have evolved later, bringing forth the ground plan that enabled expansions into a diversity of bilaterian brains and a corresponding range of complex behavioral repertoires.

References

1. Bicknell, R. D. C., Campione, N. E., Brock, G. A. & Paterson, J. R. Adaptive responses in Cambrian predator and prey highlight the arms race during the rise of animals. *Curr. Biol.* **35**, 882–888.e2 (2025).
2. Monk, T. & Paulin, M. G. Predation and the origin of neurones. *Brain Behav. Evol.* **84**, 246–261 (2014).
3. Vinn, O. Traces of predation in the Cambrian. *Hist. Biol.* **30**, 1043–1049 (2018).
4. Laing, B. A. *et al.* Remember when? Deciphering Ediacaran-Cambrian Metazoan behaviour and temporal memory using fossil movement paths. *arXiv [physics.bio-ph]* (2025).
5. Hsieh, S., Plotnick, R. E. & Bush, A. M. The Phanerozoic aftermath of the Cambrian information revolution: sensory and cognitive complexity in marine faunas. *Paleobiology* **48**, 397–419 (2022).
6. Trestman, M. The Cambrian explosion and the origins of embodied cognition. *Biol. Theory* **8**, 80–92 (2013).
7. Pagán, O. R. The brain: a concept in flux. *Philos. Trans. R. Soc. Lond. B Biol. Sci.* **374**, 20180383 (2019).
8. Richter, S. *et al.* Invertebrate neurophylogeny: suggested terms and definitions for a neuroanatomical glossary. *Front. Zool.* **7**, 29 (2010).
9. Arendt, D., Tosches, M. A. & Marlow, H. From nerve net to nerve ring, nerve cord and brain--evolution of the nervous system. *Nat. Rev. Neurosci.* **17**, 61–72 (2016).
10. Northcutt, R. G. Evolution of centralized nervous systems: Two schools of evolutionary thought. *Proceedings of the National Academy of Sciences* **109**, 10626–10633 (2012).
11. Martinez, P. & Sprecher, S. G. Of Circuits and Brains: The Origin and Diversification of Neural Architectures. *Frontiers in Ecology and Evolution* **8**, (2020).
12. Kandel, E. R., Schwartz, J. H., Jessell, T. M., Siegelbaum, S. A. & Hudspeth, A. J. *Principles of Neural Science, Fifth Edition (Principles of Neural Science (Kandel))*. 1760

(McGraw-Hill Medical, 2012).

13. Szczepanski, S. M. & Knight, R. T. Insights into human behavior from lesions to the prefrontal cortex. *Neuron* **83**, 1002–1018 (2014).

14. Carlisle, E., Yin, Z., Pisani, D. & Donoghue, P. C. J. Ediacaran origin and Ediacaran-Cambrian diversification of Metazoa. *Sci. Adv.* **10**, eadp7161 (2024).

15. Budd, G. E. & Mann, R. P. Two notorious nodes: A critical examination of relaxed molecular clock age estimates of the bilaterian animals and placental mammals. *Syst. Biol.* **73**, 223–234 (2024).

16. Arendt, D. Elementary nervous systems. *Philos. Trans. R. Soc. Lond. B Biol. Sci.* **376**, 20200347 (2021).

17. Romanes, G. J. XI. The Croonian lecture.--Preliminary observations on the locomotor system of medusæ. *Philos. Trans. R. Soc. Lond.* **166**, 269–313 (1876).

18. Anctil, M. *Dawn of the Neuron*. (McGill-Queen's University Press, Montréal, QC, Canada, 2015).

19. Courtney, A. *et al.* Characterization of geometric variance in the epithelial nerve net of the ctenophore Pleurobrachia pileus. *J. Comp. Neurol.* **530**, 1438–1458 (2022).

20. Mackie, G. O. The first description of nerves in a cnidarian: Louis Agassiz's account of 1850. in *Coelenterate Biology 2003* 27–32 (Springer Netherlands, Dordrecht, 2007).

21. Weissbourd, B. *et al.* A genetically tractable jellyfish model for systems and evolutionary neuroscience. *Cell* **184**, 5854–5868.e20 (2021).

22. Dupre, C. & Yuste, R. Non-overlapping Neural Networks in Hydra vulgaris. *Curr. Biol.* **27**, 1085–1097 (2017).

23. Jékely, G. & Yuste, R. Nonsynaptic encoding of behavior by neuropeptides. *Curr. Opin. Behav. Sci.* **60**, 101456 (2024).

24. Anderson, P. A. & Spencer, A. N. The importance of cnidarian synapses for neurobiology. *J. Neurobiol.* **20**, 435–457 (1989).

25. Satterlie, R. A. Cnidarian Nerve Nets and Neuromuscular Efficiency. *Integr. Comp. Biol.* **55**, 1050–1057 (2015).
26. Burkhardt, P. *et al.* Syncytial nerve net in a ctenophore adds insights on the evolution of nervous systems. *Science* **380**, 293–297 (2023).
27. Jokura, K., Jasek, S., Niederhaus, L., Burkhardt, P. & Jékely, G. Neural Connectome of the Ctenophore Statocyst. (2025) doi:10.7554/elife.108420.
28. Holland, N. D. Early central nervous system evolution: an era of skin brains? *Nat. Rev. Neurosci.* **4**, 617–627 (2003).
29. Álvarez-Presas, M., Ruiz-Trillo, I. & Paps, J. Novel genomic approaches support Xenacoelomorpha as sister to all Bilateria. *Research Square* (2024) doi:10.21203/rs.3.rs-5529390/v1.
30. Cannon, J. T. *et al.* Xenacoelomorpha is the sister group to Nephrozoa. *Nature* **530**, 89–93 (2016).
31. Srivastava, M., Mazza-Curll, K. L., van Wolfswinkel, J. C. & Reddien, P. W. Whole-Body Acoel Regeneration Is Controlled by Wnt and Bmp-Admp Signaling. *Curr. Biol.* **24**, 1107–1113 (2014).
32. Philippe, H. *et al.* Acoelomorph flatworms are deuterostomes related to Xenoturbella. *Nature* **470**, 255–258 (2011).
33. Reuter, M. *et al.* Organisation of the nervous system in the Acoela: an immunocytochemical study. *Tissue Cell* **33**, 119–128 (2001).
34. Hejnol, A. & Martindale, M. Q. Acoel development supports a simple planula-like urbilaterian. *Philos. Trans. R. Soc. Lond. B Biol. Sci.* **363**, 1493–1501 (2008).
35. Bourlat, S. J. & Hejnol, A. Acoels. *Curr. Biol.* **19**, R279–280 (2009).
36. Hulett, R. E., Potter, D. & Srivastava, M. Neural architecture and regeneration in the acoel Hofstenia miamia. *Proc. Biol. Sci.* **287**, 20201198 (2020).
37. Achatz, J. G. & Martinez, P. The nervous system of Isodiametra pulchra (Acoela) with a

537 discussion on the neuroanatomy of the Xenacoelomorpha and its evolutionary implications.
538 *Front. Zool.* **9**, 27 (2012).
539 38. Hooge, M. *et al.* A revision of the systematics of panther worms (Hofstenia spp., Acoela),
540 with notes on color variation and genetic variation within the genus. *Hydrobiologia* **592**,
541 439–454 (2007).
542 39. Corrêa, D. D. Two New Marine Turbellaria from Florida. *Bull. Mar. Sci.* **10**, 208–216 (1960).
543 40. Bock, S. *Eine Neue Marine Turbellariengattung Aus Japan*. (Almqvist & Wiksell, 1923).
544 41. Steinböck, O. Grundsätzliches zur Evolution der Turbellarien. *Zeitschrift für Zoologische*
545 *Systematik und Evolutionsforschung* **4**, 58–195 (1966).
546 42. Chandra, V., Tseng, S. E., Kann, A. P., Marcela Bolanos, D. & Srivastava, M.
547 Developmental, regenerative, and behavioral dynamics in acoel reproduction. *Elife*
548 RP105712 (2025).
549 43. Todt, C. & Tyler, S. Ciliary receptors associated with the mouth and pharynx of Acoela
550 (Acoelomorpha): a comparative ultrastructural study: Ciliary receptors of Acoela. *Acta Zool.*
551 **88**, 41–58 (2006).
552 44. Keramidioti, A. *et al.* A new look at the architecture and dynamics of the Hydra nerve net.
553 *Elife* **12**, (2024).
554 45. Zhang, S. *et al.* Ultrastructural reconstruction of the endodermal nerve net of Hydra
555 vulgaris. *Curr. Biol.* **35**, 5490–5501.e3 (2025).
556 46. Bullock, T. H. & Horridge, G. A. *Structure and Function in the Nervous Systems of*
557 *Invertebrates*. (W.H. Freeman, New York, NY, 1965).
558 47. Scheffer, L. K. *et al.* A connectome and analysis of the adult Drosophila central brain. *Elife*
559 **9**, (2020).
560 48. Montague, T. G. *et al.* A brain atlas for the camouflaging dwarf cuttlefish, Sepia bandensis.
561 *Curr. Biol.* **33**, 2794–2801.e3 (2023).
562 49. Anderson, D. J. & Adolphs, R. A framework for studying emotions across species. *Cell* **157**,

563 187–200 (2014).
564 50. Kann, A. P. & Srivastava, M. Cooperation between proximate cell layers drives large-scale
565 wound closure prior to whole-body regeneration. *bioRxivorg* (2025)
566 doi:10.1101/2025.02.03.636261.
567 51. Ricci, L. & Srivastava, M. Transgenesis in the acoel worm Hofstenia miamia. *Dev. Cell* **56**,
568 3160–3170.e4 (2021).
569 52. Büschges, A., Scholz, H. & El Manira, A. New moves in motor control. *Curr. Biol.* **21**, R513–
570 24 (2011).
571 53. Büschges, A. & Ache, J. M. Motor control on the move: from insights in insects to general
572 mechanisms. *Physiol. Rev.* **105**, 975–1031 (2025).
573 54. Hulett, R. E. *et al.* Acoel single-cell atlas reveals expression dynamics and heterogeneity of
574 adult pluripotent stem cells. *Nat. Commun.* **14**, 2612 (2023).
575 55. Hulett, R. E., Rivera-López, C., Gehrke, A. R., Gompers, A. & Srivastava, M. A wound-
576 induced differentiation trajectory for neurons. *Proc. Natl. Acad. Sci. U. S. A.* **121**,
577 e2322864121 (2024).
578 56. Court, R. *et al.* Virtual Fly Brain-An interactive atlas of the Drosophila nervous system.
579 *Front. Physiol.* **14**, 1076533 (2023).
580 57. Shainer, I. *et al.* A single-cell resolution gene expression atlas of the larval zebrafish brain.
581 *Sci. Adv.* **9**, eade9909 (2023).
582 58. Rock, A. Q. & Srivastava, M. Totipotency and high plasticity in an embryo with a
583 stereotyped, invariant cleavage program. *bioRxivorg* (2025)
584 doi:10.1101/2025.02.12.637942.
585 59. Goulty, M., Botton-Amiot, G., Rosato, E., Sprecher, S. G. & Feuda, R. The monoaminergic
586 system is a bilaterian innovation. *Nat. Commun.* **14**, 3284 (2023).
587 60. Thiel, D., Franz-Wachtel, M., Aguilera, F. & Hejnol, A. Xenacoelomorph neuropeptidomes
588 reveal a major expansion of neuropeptide systems during early bilaterian evolution. *Mol.*

589 *Biol. Evol.* **35**, 2528–2543 (2018).
590 61. Hsiao, J., Deng, L. C., Chalasani, S. & Edsinger, E. Numerous expansions in TRP ion
591 channel diversity highlight widespread evolution of molecular sensors in animal
592 diversification. *bioRxiv* 2021.11.14.466824 (2021) doi:10.1101/2021.11.14.466824.
593 62. Lashley, K. S. *Brain Mechanisms and Intelligence: A Quantitative Study of Injuries to the*
594 *Brain*. vol. 186 (University of Chicago Press, Chicago, 1929).
595 63. Nadel, L. & Maurer, A. P. Recalling Lashley and reconsolidating Hebb. *Hippocampus* **30**,
596 776–793 (2020).
597 64. Petersen, S. E., Seitzman, B. A., Nelson, S. M., Wig, G. S. & Gordon, E. M. Principles of
598 cortical areas and their implications for neuroimaging. *Neuron* (2024)
599 doi:10.1016/j.neuron.2024.05.008.
600 65. Makin, T. R. & Krakauer, J. W. Against cortical reorganisation. *eLife* **12**, e84716 (2023).
601 66. Kolb, B. & Whishaw, I. Q. Mass Action and Equipotentiality Reconsidered. in *Brain Injury*
602 *and Recovery: Theoretical and Controversial Issues* (eds. Finger, S., Levere, T. E., Almli,
603 C. R. & Stein, D. G.) 103–116 (Springer US, Boston, MA, 1988).
604 67. Hejnol, A. & Lowe, C. J. Embracing the comparative approach: how robust phylogenies and
605 broader developmental sampling impacts the understanding of nervous system evolution.
606 *Philos. Trans. R. Soc. Lond. B Biol. Sci.* **370**, (2015).
607 68. Ferraioli, A. *et al.* The 3D architecture of the ctenophore aboral organ and the evolution of
608 complex integrative centers in animals. *bioRxiv* 2025.06.26.659588 (2025)
609 doi:10.1101/2025.06.26.659588.
610 69. Grimmelikhuijzen, C. J. & Westfall, J. A. The nervous systems of cnidarians. *EXS* **72**, 7–24
611 (1995).
612 70. Breen, C. & Srivastava, M. A spreading, multi-tissue wound signal initiates whole-body
613 regeneration. *bioRxiv* (2024) doi:10.1101/2024.12.10.627832.
614 71. Baena, V., Schalek, R. L., Lichtman, J. W. & Terasaki, M. Serial-section electron

615 microscopy using automated tape-collecting ultramicrotome (ATUM). *Methods Cell Biol.*
616 **152**, 41–67 (2019).
617 72. Pachitariu, M., Rariden, M. & Stringer, C. Cellpose-SAM: superhuman generalization for
618 cellular segmentation. *bioRxiv* 2025.04.28.651001 (2025) doi:10.1101/2025.04.28.651001.
619 73. Pearson, B. J. *et al.* Formaldehyde-based whole-mount in situ hybridization method for
620 planarians. *Dev. Dyn.* **238**, 443–450 (2009).
621 74. Mathis, A. *et al.* DeepLabCut: markerless pose estimation of user-defined body parts with
622 deep learning. *Nat. Neurosci.* **21**, 1281–1289 (2018).
623 75. Pereira, T. D. *et al.* SLEAP: A deep learning system for multi-animal pose tracking. *Nat.*
624 *Methods* **19**, 486–495 (2022).

625

626 **Acknowledgments**

627 We thank Ugne Klibaite, Brandon Logeman, Aravinthan Samuel, David Palmer, Ishaan
628 Chandok, Aditi Chandra, Benjamin de Bivort, Madeleine Snyder, Julian Smith III, and the entire
629 Srivastava Lab for helpful discussion. We thank D. Marcela Bolanos, Samantha Tseng, and
630 Julian Kimura for assisting with data collection, Maria Ericsson and the Harvard Medical School
631 Electron Microscopy Core Facility for high-pressure freezing and sample preparation, Ed Soucy
632 and Jazz Weisman for behavioral advice, and Tim Sackton and Tommy Tang for single-cell
633 analysis advice. VC and APK are Fellows of the Jane Coffin Childs Fund for Medical Research.
634 VC acknowledges funding from the Harvard Brain Initiative's Postdoctoral Pioneer Award. AS
635 was supported by a grant from the Harvard Museum of Comparative Zoology. This project was
636 supported by an NIH BRAIN R34 award (1R34DA061984) to MS.
637

638 **Author Contributions**

639 VC and MS designed the project. VC performed behavioral experiments. VC and MRN
640 performed computational behavioral analyses. VC, APK, AS, KAPH, and RS performed
641 molecular labeling and imaging experiments. VC analyzed transcriptomic and imaging data. JL
642 enabled electron microscopy. MS and LM supervised the project. VC and MS wrote the
643 manuscript with input from all authors.

644 **Methods**

645

646 **Animal husbandry**

647 Juvenile *Hofstenia miamia* worms were reared in communal plastic tanks with artificial sea
648 water (37ppt, pH between 7.8 and 8.2), held at room temperature with an approximate day-light
649 cycle. Sea water was replaced twice weekly, and the worms were fed marine rotifers
650 (*Brachionus plicatilis*).

651

652 For behavioral experiments, worms were isolated from their culturing tanks, and placed in
653 individual wells of 6- or 12-well plates (Falcon #353046). Worms were typically 3-5 weeks post
654 hatching, at which point they varied in their sexual maturity. Preliminary observations indicated
655 that this variation did not affect foraging behavior, and each experiment was initiated with worms
656 from the same communal tank, of approximately the same age and size. Worms that were in the
657 middle stages of sexual maturity were fed rotifers, brine shrimp (*Artemia sp.*) or a mix of the two,
658 as previously described[42]. To amputate worms, we anesthetized them in 15% tricaine (ethyl 3-
659 aminobenzoate methanesulfonic acid; Sigma #E10521) for 10-20 minutes, and amputated them
660 with micro knives (Fine Science Tools #10316-14) before washing in artificial sea water to allow
661 recovery. Control worms in these experiments were anesthetized for the same amount of time,
662 but were not amputated. For foraging experiments, worms were starved for 1-2 weeks.

663

664 **Dyes and live imaging**

665 We used several live dyes to stain *H. miamia* brains. We used the voltage dye DiBAC4(3)
666 (Invitrogen #B438) to stain the nervous system. We dissolved DiBAC4(3) in pure ethanol to
667 create a 1mg/ml stock solution. We diluted this 1:1000 in artificial sea water with 15% tricaine.
668 Worms were incubated in this solution for 30 min. They were then mounted in a gel of 2%
669 methylcellulose (in artificial sea water containing 15% tricaine) on a glass slide, compressed
670 under a glass coverslip with clay feet, and imaged. The calcium dye ICR-1 AM (Ion Biosciences
671 #1091F) was reconstituted in DMSO and then diluted in artificial sea water with 15% tricaine to
672 a concentration of 40μM. Worms were incubated in this solution for 1-2hrs, then mounted on a
673 glass slide in methylcellulose, using the same procedure as above. SiR-Tubulin (Cytoskeleton,
674 CY-SC002) was dissolved in 50μL DMSO according to manufacturer instructions, then worms
675 were incubated in a 1:1000 solution in artificial sea water with 15% tricaine for 90m prior to
676 mounting as described above. *Troponin::Kaede* animals, described previously[51], were
677 anesthetized in tricaine, and mounted using the same procedures as above.

678

679 **Irradiation**

680 To kill adult pluripotent stem cells, seven days before amputation, worms were exposed to
681 gamma radiation for a total dose of 10000 rad. Worms were then amputated and their behavior
682 was assayed two days later as described below. All worms survived irradiation.

683

684 **Immunofluorescence**

685 We performed immunofluorescence using previously described protocols[42]. Briefly, worms were
686 fixed in 4% paraformaldehyde in artificial sea water for 1h at room temperature. Fixed animals
687 were washed in PBST (PBS + 0.1% Triton-X-100) three times, then blocked in 10% goat serum
688 (ThermoFisher, #16210072) in PBST for 1h at room temperature. Samples were incubated in
689 primary antibodies in blocking solution for 48h at 4°C, washed thoroughly (6x 20 minutes) in
690 PBST, incubated in blocking solution for 1h at room temperature, then incubated in secondary
691 antibody overnight at 4°C. Animals were washed thoroughly once more (6x 20 minutes) in
692 PBST, then counterstained with Hoechst 33342 and SiR-actin (where applicable). All steps were
693 carried out on an orbital shaker. Primary antibodies used: Par3 (St. John's Laboratory
694 #STJ94951, 1:200), β-catenin (Fisher Scientific #RB9035P0, 1:200), pERK (Cell Signaling
695 Technologies #4370T, 1:200) [70], FMRFamide (EMDMillipore #AB15348, 1:1000)[36].
696 Counterstains used: Hoechst 33342 (ThermoFisher #62249, 1:800) and SiR-actin (Cytoskeleton
697 #CY-SC001, 1:1000)[50]. Goat anti-Rabbit IgG (H+L) Cross-Adsorbed Secondary Antibody, Alexa
698 Fluor™ 568 (ThermoFisher #A-11011, 1:800) was used as a secondary antibody.
699
700 **Electron Microscopy**
701 We fixed hatchling juvenile worms using high-pressure fixation. A mix of intact worms and
702 amputated heads in 15% tricaine in artificial sea water were placed in 100μm-tall aluminium
703 planchettes, and were rapidly frozen in liquid nitrogen using a Leica EM ICE high-pressure
704 freezing instrument. These planchettes were then transferred under liquid nitrogen into cryovials
705 containing a freeze substitution cocktail (1% OsO4 and 0.1% uranyl acetate). Freeze
706 substitution involved holding the cryovials at -90°C for 36-48h, followed by warming up to -60°C
707 over 6h and holding for 6h, warming up to -30°C over 6h and holding for 3h, warming up to 0°C
708 over 6h and holding for 1h, and finally warming up to room temperature over 4h. Specimens
709 were then rinsed in acetone three times for 10m each. They were then extracted from the
710 planchettes and embedded in an Epon-Araldite resin. Resin blocks were baked at 60°C for 48h,
711 after which they were sectioned with a Leica UC6 ultramicrotome using a DiATOME diamond
712 knife, and collected onto tape using ATUM[71]. Sections of tape were then mounted on silicon
713 wafers as previously described[71], and were imaged using a Zeiss Sigma scanning electron
714 microscope. Neurites in Fig. 1j,k were segmented using Cellpose-SAM[72] with manual correction.
715
716 **Riboprobe synthesis and fluorescence *in situ* hybridization (FISH)**
717 We performed FISH using protocols described previously[31,73], with minor modifications. Briefly,
718 we used nested PCR to extract template sequences from cDNA. Riboprobes were synthesized
719 from these templates using a digoxigenin (DIG) labeling mix, as previously described[31,73].
720 Worms were starved for 1-2 weeks prior to fixation to ensure that their guts were empty. They
721 were then fixed in 4% paraformaldehyde in artificial sea water for one hour at room temperature.
722 We washed worms in PBST (PBS + 0.1% Triton-X-100), 50% PBST/50% MeOH solution, and
723 chilled MeOH for 5m each. They were then transferred to baskets in 24-well plates containing
724 800μL of solution per well, washed once in 50% MeOH/50% PBST, then twice in PBST. To
725 remove pigmentation and autofluorescence, they were bleached in a solution of 88.5% MilliQ

726 water, 4% hydrogen peroxide, 2.5% 20X SSC, and 5% formamide, then washed in PBST twice.
727 Worms were then incubated for 10 minutes in Proteinase K solution (0.1% SDS, 0.9% MilliQ
728 water, and 0.01% Proteinase K in PBST), post-fixed in formaldehyde solution (4% formaldehyde
729 in PBST) for 10m, and washed in PBST. They were then incubated in 50% PBST/50% PreHyb
730 (50% DI Formamide, 25% 20X SSC, 0.5% Tween-20, 24.5% MilliQ water, 0.001g/mL Yeast
731 RNA), transferred to 100% PreHyb and incubated at 56°C for 2hrs. 1μL of probe was then
732 mixed with 799μL of hybridization solution (50% DI Formamide, 25% 20X SSC, 0.5% Tween-20,
733 5% dextran sulfate, 19.5% MilliQ water, 0.001g/mL Yeast RNA), denatured at 72°C for 5m, and
734 distributed in the wells. The worms were moved into the probe solution, sealed, and incubated
735 at 56°C overnight. The following day, the worms were washed twice in PreHyb, twice in 50%
736 PreHyb/50% 2X SSCT (10% 20X SSC, 0.1% TritonX-100, 89.9% MilliQ water), 100% 2X SSCT,
737 then 0.2X SSCT (1% 20X SSC, 0.1% TritonX-100, 98.9% MilliQ water), for 30m each at 56°C.
738 They were then cooled at room temperature for 10mins, washed in PBST, incubated in blocking
739 solution for 1hr (90% PBST, 5% horse serum, and 5% 10X Casein), then moved to 1:1500
740 blocking solution:Anti-DIG, sealed, and left at 4°C overnight. The next day they were washed six
741 times for 20m each in PBST, incubated in tyramide buffer for 10m, then development solution
742 (0.1% rhodamine, 0.1% IPBA, and 0.01% H2O2 in tyramide buffer) for 10m. They were then
743 washed in PBST 3 times before being moved to a solution of 1:500 Hoechst 33342
744 (ThermoFisher #62249) in PBST, sealed, and left at 4°C overnight. Finally, they were washed in
745 PBST, and then mounted on glass slides in VECTASHIELD® PLUS Antifade Mounting Medium
746 (Vector Laboratories, H-1900). All steps except the 56°C incubations were carried out using an
747 orbital shaker.
748
749 **FISH analysis**
750 We collected all images with a Leica SP8 point-scanning confocal microscope. 3D images of
751 FISH-labeled neural markers in brains were generally acquired through a 20x objective. We
752 then generated a maximum intensity z-projection of the brain for each of these images, and
753 trained a supervised pixel classifier in ilastik to segment pixels that had FISH signal. These
754 binary images were then smoothed in FIJI through a process of erosion and hole filling, before
755 computational analysis.
756 To quantify regionalization of neural markers within the brain, we computed two indices
757 of regionalization. First, we partitioned each brain into a heatmap containing 25 pixels, and we
758 calculated the proportion of pixels containing fluorescent puncta. We then calculated the Gini
759 coefficient (a standard measure of inequality) of each heatmap. To correct for differences in
760 regionalization expected as an artifact of sparseness, we simulated brains with uniformly
761 distributed fluorescent puncta of the same sparseness. Computing the difference in Gini
762 coefficients between real and matched simulated brains provided a robust index of
763 regionalization. Second, for each brain we constructed the convex hull of the set of fluorescent
764 puncta positions, treating puncta as points in the imaging plane. We computed the area
765 enclosed by this convex hull and normalized it by the area of the polygon defining the brain
766 boundary, yielding a dimensionless coverage ratio that quantifies the spatial extent of puncta

767 relative to the entire brain. To generate a second index of regionalization, we measured the
768 difference between real ratios and corresponding ratios within simulated brains with uniformly
769 distributed puncta.
770
771 **Behavior**
772 **Behavioral imaging**
773 All behavioral experiments were conducted in 6-well plates filmed with 850nm infrared side-
774 lighting from two LED strips behind a white acrylic diffuser (McMaster-Carr #8505K741), within a
775 custom behavioral chamber shielded from visible light. The chamber was cooled with a USB fan
776 to maintain temperatures between 22 and 25°C. Experiments were filmed in parallel using four
777 machine vision cameras (FLIR Blackfly BFS-U3-120S4M-CS and Basler Ace ac4024-29um
778 USB 3.0 monochrome, with Tamron M118FM16 16mm lenses) at 12 megapixels and 10Hz for
779 1h, streaming to a custom-built desktop computer; each video contained four or six wells of a
780 single plate within its field of view. We then used a custom MATLAB script for pre-processing:
781 background subtraction, contrast enhancement, and cropping the video into a set of separate
782 output videos for each well of the plate. We typically scaled videos to a resolution of 1000x1000
783 pixels, masking areas outside the arenas, and aligning their centers to make xy coordinates
784 comparable across videos.
785
786 **Immobilized rotifer foraging assay**
787 To study the foraging behavior of *H. miamia* presented with immobilized prey, we developed an
788 assay to present worms a choice between blocks of agarose that either did or did not contain
789 groups of live, immobilized rotifers. Rotifers were embedded in ~1% agarose blocks using the
790 following protocol. For each agarose block, 100μL of a well-mixed stock solution of rotifers (on
791 the order of thousands of rotifers per mL) or 100μL of artificial sea water for controls, was first
792 aliquoted into the bottom of a subset of wells of a 96-well plate. 100μL of hot 2% UltraPure Low
793 Melting Point agarose (Invitrogen #16520-100) was then added immediately above. The plate
794 was then cooled at 4°C for 30m. Each solid agarose block was then placed against the wall of a
795 well of a 6-well plate, with a block of agarose alone and a block of agarose containing rotifers at
796 opposite ends of the wall. A small volume of 2% agarose was then pipetted onto this block to
797 glue it to the wall of the plate. 5-10m later, 6ml of artificial sea water was pipetted into the well, a
798 single *H. miamia* worm was introduced to the well and the behavioral experiment initiated.
799
800 **Tracking and foraging analysis**
801 We trained custom models in DeepLabCut[74] and SLEAP[75] to track keypoints on the worm. To
802 study foraging behavior, we quantified the position and movement of worm centroids inferred
803 from these keypoints. We systematically excluded worms from the analysis if they were tracked
804 poorly, or which were inactive for sustained periods over the course of the experiment (a
805 minority of worms fit these exclusion criteria across our experiments, independent of their
806 feeding or amputation status). To quantify the proportion of time spent near food (i.e. rotifers

embedded in agarose), we defined an experiment-specific threshold distance, and quantified the proportion of frames in which the worm was within that distance.

Postural analysis

For the datasets used for postural analysis, we tracked seven keypoints along the midline of the worm. We smoothed the xy coordinates of these points, used median-filling to remove NaNs, and then fit a 20-jointed spline to this data. Preliminary observations of the worms suggested that their postural dynamics are well represented by three features: the curvature of their midlines, their body lengths, and the speeds the worms travel at. We calculated the curvature of the spline as the normalized ratio of the sum of the lengths of its segments to the length between the first and last points. This ratio was scaled to lie within the range [-1,1], where -1 represented a sharp left bend, 0 represented the worm's posture when straight, and 1 represented a sharp right bend. Worm length was calculated as the sum of the segments composing the spline; this was z-scored to enable comparison across worms and across experiments in which the measured length varied slightly as a function of precise camera parameters. Speed was calculated as minimum displacement between splines in consecutive frames. All measures were smoothed and filtered to remove outliers. We used PCA to reduce this curvature-length-speed space to 2D; we then used k-means clustering to partition this postural space into elemental postures as described in the text. We used multiple large language models to assist with generating analysis code.

Single-cell RNA sequencing analysis

We integrated single-cell RNA sequencing libraries from three previous sequencing experiments. These included worms that ranged from hatchlings (i.e. juvenile worms that have just emerged from their egg shells) to adults, and worms in various stages of regeneration after a transverse amputation. We re-aligned these libraries to an updated transcriptome[58]. We then regressed library identity to correct for batch effects, identified neural clusters, extracted and re-clustered neural cells.

Hunting behavior assay and analysis

To study the behavior of *H. miamia* actively hunting escaping prey, we introduced a single worm and a single brine shrimp to each well of a 6-well plate. We filmed these arenas for 1h at 10Hz in infrared lighting conditions, using the imaging parameters described above.

We then tracked worms and brine shrimp using custom-trained SLEAP models. To find the velocity of the worm at frame i while smoothing tracking noise, we averaged the center-of-mass velocity over five frames before and after frame i. The velocity correlation function was then calculated for the entire trajectory of each sample using the definition $\langle v_w(t+\Delta t) \cdot v_w(t) \rangle_t$, where $v_w(t)$ denotes the velocity of the worm at time t, and the average is taken over time t. The final velocity correlation function shown in Fig. S7d is obtained by averaging the velocity correlation functions of worms across different experiments with the same treatment.

To quantify the correlation between the velocity of the worm and the trajectory of the shrimp (Fig.4d,e; Fig. S7e), we used the smoothed worm velocity v_v and calculated its correlation with the vector connecting the worm's position to the shrimp's position in earlier frames. The correlation is defined as $\langle v_w(t) \cdot \Delta r_{v_{sh}}(t-\Delta t)\rangle_t$, where $\Delta r_{v_{sh}}(t-\Delta t)$ is the unit vector pointing from the worm at time t to the shrimp at time t-Δt.